

# Polymer Chemistry

Accepted Manuscript



This is an *Accepted Manuscript*, which has been through the Royal Society of Chemistry peer review process and has been accepted for publication.

*Accepted Manuscripts* are published online shortly after acceptance, before technical editing, formatting and proof reading. Using this free service, authors can make their results available to the community, in citable form, before we publish the edited article. We will replace this *Accepted Manuscript* with the edited and formatted *Advance Article* as soon as it is available.

You can find more information about *Accepted Manuscripts* in the [Information for Authors](#).

Please note that technical editing may introduce minor changes to the text and/or graphics, which may alter content. The journal's standard [Terms & Conditions](#) and the [Ethical guidelines](#) still apply. In no event shall the Royal Society of Chemistry be held responsible for any errors or omissions in this *Accepted Manuscript* or any consequences arising from the use of any information it contains.

Cite this: DOI: 10.1039/c0xx00000x

www.rsc.org/xxxxxx

ARTICLE

# Low band-gap copolymer composed of thienyl substituted anthracene and diketopyrrolopyrrole compatible with multiple electron acceptors for high efficiency polymer solar cells

Jae Woong Jung<sup>a</sup> and Won Ho Jo<sup>a</sup>

Received (in XXX, XXX) Xth XXXXXXXXX 20XX, Accepted Xth XXXXXXXXX 20XX  
DOI: 10.1039/b000000x

A low band-gap copolymer consisting of 9,10-thienyl-substituted anthracene (TA) as an electron-donating unit and diketopyrrolopyrrole (DPP) as an electron-withdrawing unit has been synthesized and applied to the donor material in polymer solar cells. The weak electron-donating characteristic of TA, which has 2-D extended conjugation by thiophene side groups, makes the copolymer exhibit a low-lying HOMO level of  $-5.5$  eV with a low band-gap of  $1.65$  eV, which affords both high photo-voltage and photo-current of the polymer solar cells. As a result, the solar cell device fabricated from the blend of the copolymer and PC<sub>71</sub>BM exhibits a promising power conversion efficiency of  $7.02\%$  ( $V_{OC} = 0.80$  V,  $J_{SC} = 13.1$  mA/cm<sup>2</sup>, FF =  $0.67$ ). Moreover, the polymer solar cell as fabricated from the blend of the copolymer and di-perylene bisimide (di-PBI) as a non-fullerene electron acceptor exhibits a promising power conversion efficiency of  $4.23\%$  with  $V_{OC} = 0.77$  V,  $J_{SC} = 9.8$  mA/cm<sup>2</sup>, FF =  $0.56$ . This photovoltaic performance of the copolymer not only demonstrates that the TA is a promising electron-donating building block for high performance low band-gap copolymer, but also the copolymer is compatible with both PC<sub>71</sub>BM and non-fullerene acceptor for high efficiency polymer solar cells.

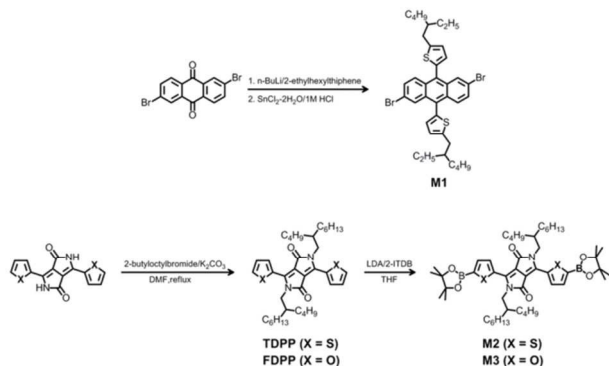
## Introduction

Polymer solar cells (PSCs) have important advantages over inorganic-based solar cells such as low material-cost, ease of fabrication with low processing-cost and the potential for fabrication of large area and flexible solar cells.<sup>1</sup> For the last decade, a remarkable progress in the performance of PSCs has been achieved by introducing bulk heterojunction (BHJ) structure in the active layer.<sup>2–5</sup> It has also been demonstrated that low band-gap conjugated polymers with broad absorption of the solar spectrum are promising active layer materials to achieve high power conversion efficiency (PCE).<sup>6,7</sup> Hence, an effective approach to achieve high PCE of PSC is to design and synthesize high performance conjugated polymers.<sup>8–11</sup> In recent efforts to develop high performance conjugated polymers, building blocks are carefully designed for the conjugated polymers to have adequate energy level, broad light absorption and strong self-assembly for use in BHJ PSC.<sup>12–18</sup>

As one of the most promising building blocks for constructing low band-gap conjugated polymers, diketopyrrolopyrrole (DPP) have emerged as the desirable electron-withdrawing moiety.<sup>19,20</sup> For the past five years, a variety of conjugated polymers containing DPP have been investigated as promising semiconductors for application in organic optoelectronics such as field effect transistors, memory devices and PSCs. Indeed, DPP-based conjugated polymers have achieved impressive PCEs up to  $9\%$  by combination of DPP and various electron-donating building blocks.<sup>21–25</sup> On the other hand, fused heteroarenes have

been utilized as an electron-donating unit for synthesis of DPP-based conjugated polymers. The incorporation of extended fused aromatic unit in polymer backbone is expected to induce strong intermolecular interactions ( $\pi$ - $\pi$  stacking), affording high crystallinity to the polymer and thus resulting in reduced energy barrier for charge carrier transport. Therefore, the DPP-based copolymers combined with fused heteroarenes have shown low band-gaps with excellent charge transport characteristics and thus high short circuit current density ( $J_{SC}$ ) of the solar cell device.<sup>26–29</sup> However, since low band-gap DPP-based copolymers usually exhibit relatively high-lying highest occupied molecular orbital (HOMO) energy level, leading to low open circuit voltage ( $V_{OC}$ ) of PSCs, a compromise between the band-gap and HOMO energy level of DPP-based polymer is critically required.

One way to solve the trade-off between  $V_{OC}$  and  $J_{SC}$  of the PSC based on low band-gap polymers is to introduce arene groups which have weak electron-donating power. When benzene or naphthalene group which has weak electron-donating nature was incorporated in DPP-based copolymers, low-lying HOMO energy level was achieved without large sacrifice of band-gap, and as a result PCEs were improved with enhanced  $V_{OC}$ s as compared to the counterpart polymer with strong electron-donating unit.<sup>30,31</sup> Anthracene is also an interesting building block as an electron-donating unit for low band-gap conjugated polymers, because the electron-donating power of anthracene is relatively weaker than fused heteroarenes such as thieno[3,2-*b*]thiophene and dithieno[3,2-*b*:2',3'-*d*]thiophene, and therefore anthracene-based



**Scheme 1** Synthesis of monomers for polymerization.

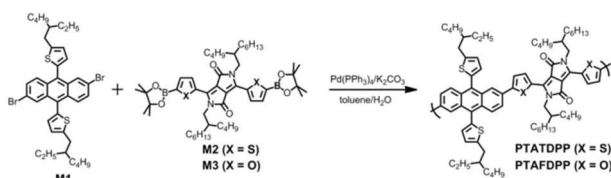
copolymer is expected to have a low-lying HOMO energy level. Furthermore, anthracene-based copolymers usually exhibit high crystallinity and high charge carrier mobility due to the coplanar fused structure of anthracene unit. Therefore, a combination of DPP and anthracene could be ideal, thus leading to high  $J_{SC}$  and  $V_{OC}$ . Nevertheless, a few studies have reported that anthracene-DPP conjugated polymers show low PCEs less than 3%.<sup>32</sup>

Here, we synthesized low band-gap copolymers incorporating 9,10-bis(5-(2-ethylhexyl)thiophen-2-yl)anthracene (TA) and DPP as electron-donating and electron-withdrawing unit, respectively. Very recently, we have successfully demonstrated that TA is a promising electron-donating moiety of medium band-gap conjugated copolymer for high performance polymer solar cells.<sup>33</sup> In conjunction with its weak electron-donating characteristics, TA possesses extended conjugation in 2-D, which is expected to enhance the light absorption and self-assembly of the resulting copolymer. Recently, it has also been reported that 2-D conjugated structure of electron-donating group in conjugated polymer is beneficial to photovoltaic properties.<sup>34</sup> Some copolymers based on 9,10-arene functionalized anthracene have recently been reported, but the absorption ranges of the polymers are limited to the wavelengths shorter than 700 nm and their PCE are moderate, 4–5%.<sup>35,36</sup> In this work, we introduced DPP with strong electron-withdrawing nature to lower the band-gap of TA-based copolymer. In addition, two different DPP derivatives flanked with thiophene (TDPP) and furan (FDPP) was used to further optimize the energy levels and photovoltaic properties of the copolymer.<sup>27</sup> Both two polymers exhibit a low band-gap of 1.65 eV, a deep HOMO energy level of  $-5.45$  eV and high hole mobility of ca.  $10^{-2}$  cm<sup>2</sup>/V·s. Interestingly, nanoscale BHJ morphology in the blend of the copolymer and PC<sub>71</sub>BM was well developed without addition of processing additive. The solar cell devices fabricated from the copolymers and PC<sub>71</sub>BM exhibited high PCEs of 7.0% and 5.2% for PTATDPP and PTAFDPP, respectively. Furthermore, the PSC fabricated from the blend of PTATDPP and non-fullerene electron acceptor (di-PBI) showed a promising PCE of 4.23%, demonstrating that PTATDPP has good

**Table 1** Characteristics of PTADPP and PTAFDPP.

| Polymer | $M_n$<br>(kDa) | PDI | $\lambda_{max}$<br>(nm) | $E_g$<br>(eV) <sup>a</sup> | HOMO<br>(eV) <sup>b</sup> | LUMO<br>(eV) <sup>b</sup> | $E_g$<br>(eV) <sup>b</sup> |
|---------|----------------|-----|-------------------------|----------------------------|---------------------------|---------------------------|----------------------------|
| PTATDPP | 47.2           | 2.1 | 654                     | 1.65                       | -5.45                     | -3.60                     | 1.85                       |
| PTAFDPP | 32.6           | 2.5 | 666                     | 1.65                       | -5.38                     | -3.45                     | 1.93                       |

<sup>a</sup> Optical band-gap. <sup>b</sup> Measured from cyclic voltammetry.



**Scheme 2** Synthesis of PTATDPP and PTAFDPP.

compatibility with multiple electron acceptors for high efficiency PSCs.

## Results and discussion

For synthesis of the copolymers, the monomer **M1** was synthesized via functionalization of 2,6-dibromo-9,10-anthraquinone by 2-(2-ethylhexyl)thiophene while **M2** and **M3** were functionalized by boronic ester for the Suzuki coupling reaction (see Scheme 1). As shown in Scheme 2, PTATDPP and PTAFDPP were synthesized by using Pd catalyst and purified by Soxhlet extraction. Both copolymers were obtained as dark purple solids in high yield over 80%, and are well soluble in common organic solvents such as chloroform, chlorobenzene and *o*-dichlorobenzene. The number-average molecular weights ( $M_n$ ) of PTATDPP and PTAFDPP were 47.2 and 32.6 kDa with polydispersity indexes (PDI) of 2.1 and 2.5, respectively, as determined by the size-exclusion chromatography.

PTATDPP and PTAFDPP show the absorption maxima ( $\lambda_{max}$ ) at 654 nm and 666 nm in solution, respectively, as shown in Figure 1a, while the two copolymers exhibit nearly the same absorption onset at 750 nm corresponding to the optical band-gap of 1.65 eV. Both copolymers also exhibit distinct vibronic shoulder peaks at 710 nm which are derived from the coupling of electronic and vibrational transition. Therefore, these vibronic shoulder peaks at lower energy provide an evidence of strong  $\pi$ - $\pi$  interaction, indicating that polymer chains are aggregated in solution state. As compared to solution state, the absorption onsets in solid state are extended to 770 nm while the vibronic shoulders become stronger, indicating that both polymer chains exhibit strong tendency to self-assemble in the solid state, which may induce crystallization.<sup>37</sup> This strong self-assembly of PTATDPP and PTAFDPP arises mainly from highly coplanar nature of polymer backbone. Therefore, the two copolymers are expected to possess high crystallinity in solid film state, which is beneficial to efficient charge transport in the device.

The HOMO/the lowest occupied molecular orbital (LUMO) energy levels of PTATDPP and PTAFDPP are  $-5.45$  eV/ $-3.60$  eV and  $-5.38$  eV/ $-3.45$  eV, respectively.

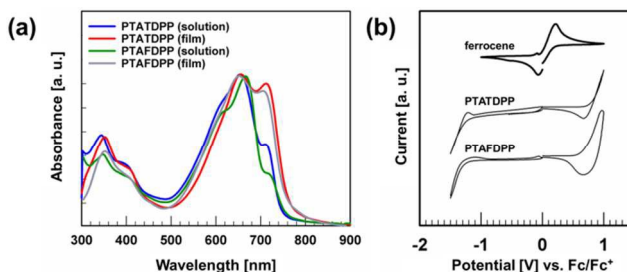


**Fig. 1** (a) UV-Vis absorption spectra and (b) cyclic voltammograms of PTATDPP and PTAFDPP.

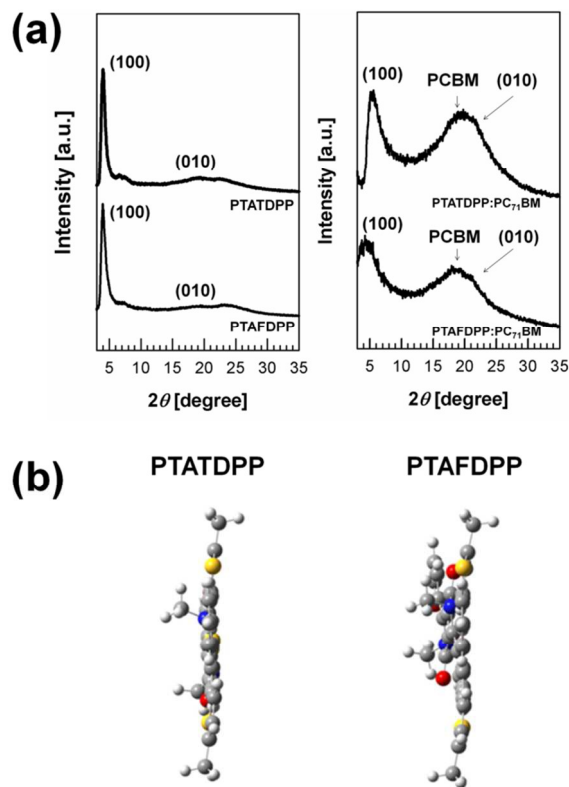


**Fig. 2** (a) X-ray diffractograms of pristine PTATDPP and PTAFDPP films (left) and their blend films with PC<sub>71</sub>BM (right), and (b) optimized structures (side view) of PTATDPP and PTAFDPP computed using the DFT at B3LYP/6-31G\* level by Gaussian03.

eV and  $-5.38$  eV/ $-3.45$  eV, respectively, as estimated from the oxidation and reduction potential of cyclic voltammograms (Fig. 1b and Table 1). The energy levels of the copolymers are lower than those of other heteroarene-based DPP copolymers reported previously,<sup>21–26</sup> and their low-lying HOMO energy levels are expected to afford high  $V_{OC}$ s of the polymer solar cells.

The crystal properties of the copolymers were investigated by X-ray diffraction (XRD). The two copolymers clearly showed a characteristic diffraction peak in range of  $3$ – $5^\circ$  with weak diffraction peak in range of  $15$ – $20^\circ$  which are associated with (100) and (010) diffraction, respectively (Figure 2a), indicating that both copolymers form crystalline lamellar structure in thin film state. It should be noted here that these copolymers exhibit distinct X-ray diffractions without any thermal treatment. Both copolymers exhibit a sharp and intense (100) diffraction peak at

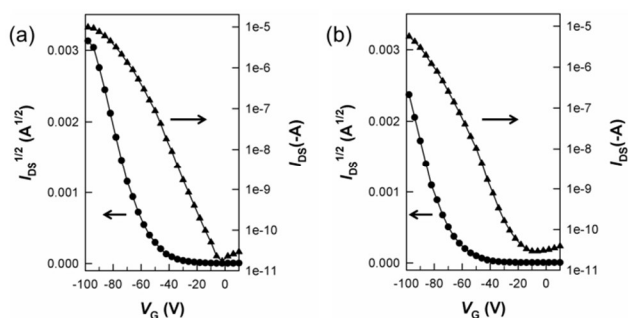


**Fig. 3** (a) Transfer characteristics of field-effect transistors with (a) PTATDPP and (b) PTAFDPP thin film.

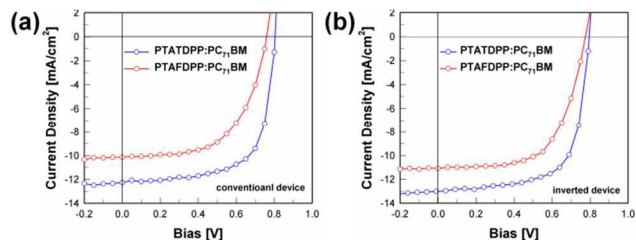


**Fig. 4**  $J$ - $V$  curves of solar cell devices fabricated from PTATDPP:PC<sub>71</sub>BM and PTAFDPP:PC<sub>71</sub>BM blends with (a) conventional and (b) inverted device architecture.

$2\theta = 4.2^\circ$  corresponding to the interchain distance ( $d_{100}$ ) of  $21.0$  Å, while the (010) diffraction peak was observed at  $19.4^\circ$  for PTATDPP and  $19.1^\circ$  for PTAFDPP, corresponding to the  $\pi$ - $\pi$  stacking distance ( $d_{010}$ ) of  $4.6$  Å and  $4.7$  Å, respectively. For identifying the reason for high crystallinity of the copolymers, the density functional theory (DFT) calculation for the minimum energy conformations of the copolymers were performed to reveal the difference of dihedral angle between TA and DPP units in the copolymers. To simplify the calculation, one repeating unit of each polymer was used as the model compound, and long alkyl substituents were replaced by ethyl group. As shown in Figure 2b, TA and TDPP have coplanar structure with a dihedral angle smaller than  $1^\circ$  while TA and FDPP have slightly distorted structure with a dihedral angle of  $3.8^\circ$ . This difference of dihedral angle between PTATDPP and PTAFDPP accounts for the difference of  $d_{010}$ , and thus PTATDPP is expected to form more closely-packed lamellar structure than PTAFDPP.

To investigate the charge transporting characteristics of PTATDPP and PTAFDPP, bottom-gate and top-contact field-effect transistors (FETs) were fabricated. Both copolymers clearly exhibit current modulation and saturation with unipolar  $p$ -type field-effect charge transporting behavior, as shown in Figure 3. The calculated saturation hole mobilities ( $\mu_h$ ) for PTATDPP and PTAFDPP are  $2.7 \times 10^{-2}$  and  $8.9 \times 10^{-3}$  cm<sup>2</sup>/V·s, respectively, with high on/off ratios ( $>10^5$ ) and low threshold voltages ( $<20$  V). The decent hole mobilities of both copolymers can be attributed to high crystallinity of the copolymers due to highly coplanar structure of anthracene and DPP. It is also understood that the 3-fold higher charge-carrier mobility of PTATDPP than that of PTAFDPP arises from its stronger  $\pi$ - $\pi$  stacking with shorter  $d_{010}$ , as discussed above.

When photovoltaic properties of copolymers are measured using PC<sub>71</sub>BM as an electron acceptor, it is found that the optimum blend ratio of polymer:PC<sub>71</sub>BM is 1:2 to afford the best PCE of both copolymers with the conventional device architecture of ITO/PEDOT:PSS/polymer:PC<sub>71</sub>BM/Ca/Al (Figure S2 and Table S1). The best PCE was also achieved when *o*-dichlorobenzene was used as solvent and the optimum thickness for the active layer was ca. 90 nm. The current density-voltage

**Table 2** Photovoltaic parameters of optimized devices based on PTATDPP and PTAFDPP.

| Polymer | Polymer:PC <sub>71</sub> BM | Device architecture | $V_{OC}$ (V) | $J_{SC}$ (mA/cm <sup>2</sup> ) | FF   | PCE (%) <sup>a)</sup> |
|---------|-----------------------------|---------------------|--------------|--------------------------------|------|-----------------------|
| PTATDPP | 1:2                         | conventional        | 0.80         | 12.3                           | 0.68 | 6.69                  |
|         |                             | inverted            | 0.80         | 13.1                           | 0.67 | 7.02                  |
| PTAFDPP | 1:2                         | conventional        | 0.76         | 11.2                           | 0.59 | 5.02                  |
|         |                             | inverted            | 0.75         | 11.4                           | 0.61 | 5.22                  |

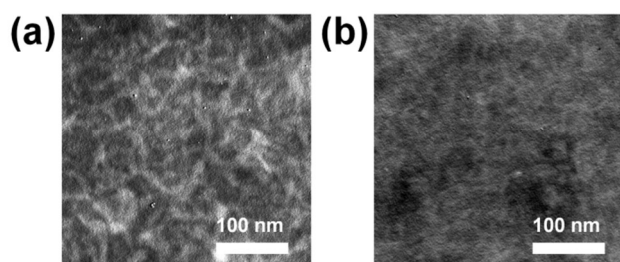


**Fig. 5** TEM images of bulk heterojunction active layers made of (a) PTATDPP:PC<sub>71</sub>BM and (b) PTAFDPP:PC<sub>71</sub>BM.

(*J*-*V*) characteristics of the optimized solar cells are shown in Figure 4, and the relevant photovoltaic parameters of the devices are summarized in Table 2 and Table S2. PTATDPP showed a best PCE of 6.69% ( $V_{OC} = 0.80$  V,  $J_{SC} = 12.3$  mA/cm<sup>2</sup>, FF = 0.68), while PTAFDPP showed a best PCE of 5.02% ( $V_{OC} = 0.76$  V,  $J_{SC} = 11.2$  mA/cm<sup>2</sup>, FF = 0.59). Both copolymers showed higher  $V_{OC}$ s than other DPP-based copolymers due to their low-lying HOMO energy levels. Both copolymers also exhibited high  $J_{SC}$ s and FFs, indicating their decent ability for charge generation and transport. Therefore, TA unit is a promising electron-donating unit for low band-gap copolymers with low-lying HOMO energy level. When the PSC devices were fabricated with inverted architecture (ITO/ZnO/polymer:PC<sub>71</sub>BM/MoO<sub>3</sub>/Ag) in order to further improve photovoltaic performance, the PCEs of PTATDPP and PTAFDPP-based devices were improved to 7.02% and 5.22%, respectively (Figure 4b, Table 2 and Table S2), mainly due to enhanced  $J_{SC}$ s ( $V_{OC}$ s and FFs were not changed significantly). It is noteworthy here that the PCE over 7% of PTATDPP is the highest efficiency of anthracene-based low band-gap conjugated copolymers.

In spite of the same band-gap of the two copolymers, PTATDPP shows slightly higher  $J_{SC}$  and FF than PTAFDPP (Figure S3). This can be ascribed to closely packed microstructure of PTATDPP and thereby its high charge-carrier mobility than PTAFDPP. When the crystal structures of blend films of the copolymers with PC<sub>71</sub>BM were examined by XRD, the PTATDPP/PC<sub>71</sub>BM blend had strong and intense (100) diffraction while the PTAFDPP/PC<sub>71</sub>BM blend showed weak and broad (100) diffraction (Figure 2b). This result leads us to conclude that PTATDPP retains higher crystalline nature in the blend with PC<sub>71</sub>BM, affording better hole transporting pathway and thus exhibiting higher  $J_{SC}$  and FF than PTAFDPP.

When the morphologies of active layers were observed by the transmission electron microscopy, the PTATDPP:PC<sub>71</sub>BM blend shows clearly fibril nanostructure (fibril width ~ 30 nm) with formation of bi-continuous network, whereas the PTAFDPP:PC<sub>71</sub>BM blend shows phase-separated morphology without formation of distinct nanostructure, as shown in Figure 5. It is well recognized that the nanoscale phase separation with fibril structure is favourable for efficient exciton dissociation and charge transport which are prerequisites for high  $J_{SC}$  and FF of PSCs. Therefore, the high FF (0.68) of PTATDPP-based device arises mainly from efficient charge-carrier mobility and formation of nanoscale fibril structure of PTATDPP.

To further evaluate the potential of PTATDPP as an electron donor material for PSCs, we fabricated non-fullerene PSC device by blending PTATDPP with a non-fullerene small molecular

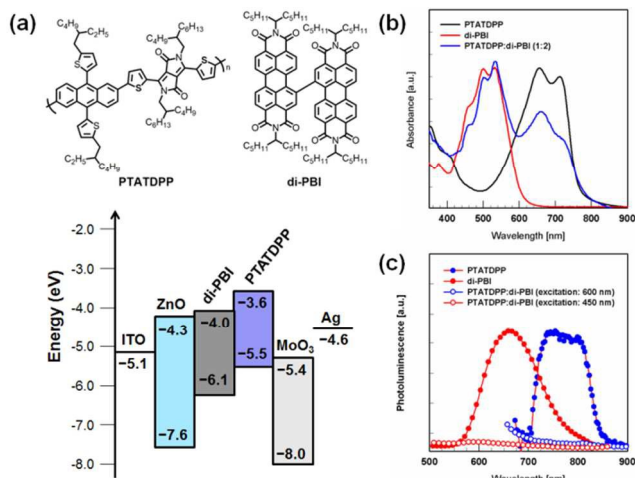


**Fig. 6** (a) Molecular structures of PTATDPP and di-PBI (top), and the schematic energy level diagram (bottom) in the PSC device based on PTATDPP and di-PBI. (b) Absorption spectra and (c) PL quenching of PTATDPP, di-PBI, and its blend films.

electron acceptor, 2,2',9,9'-tetra(undecan-6-yl)-[5,5'bianthra (2,1,9-def:6,5,10-d'e'f')diisoquinolin]-1,1',3,3',8,8',10,10'(2H,2'H,9H,9'H)-octaone (di-PBI).<sup>38</sup> As can be seen in Figure 6a, PTATDPP and di-PBI have well-matched energy levels with a LUMO-LUMO offset of 0.4 eV,<sup>39</sup> which is enough for exciton dissociation, and also exhibit complementary absorption, i.e., di-PBI and PTATDPP absorb 400–600 nm and 600–800 nm, respectively. As a consequence, the blend film (1:2 in weight ratio) exhibits broad light absorption from 400 to 800 nm. The compatibility of PTATDPP and di-PBI as electron donor and acceptor, respectively, was also examined by monitoring the photoluminescence (PL) quenching of each compound in the blend film. As shown in Figure 6c, the blend film shows excellent PL quenching over 95% of each PL from PTATDPP and di-PBI, indicating that photogenerated excitons from both PTATDPP and di-PBI are readily dissociated into free carriers at the interface of two materials.

The non-fullerene PSC fabricated from the blend of PTATDPP and di-PBI exhibits a PCE of 4.23% with  $V_{OC} = 0.77$  V,  $J_{SC} = 9.8$  mA/cm<sup>2</sup> and FF = 0.56 (Figure 7). Interestingly, the blend morphology of PTATDPP and di-PDI as observed from the atomic force microscopy (AFM) and TEM reveals that PTATDPP forms well-developed interconnected BHJ morphology with fibrillar nanostructure (Figure S4 and S5). This fibril morphology affords effective exciton dissociation as observed from PL quenching experiment. Although the non-fullerene PSC exhibits lower PCE than the PC<sub>71</sub>BM-based device,

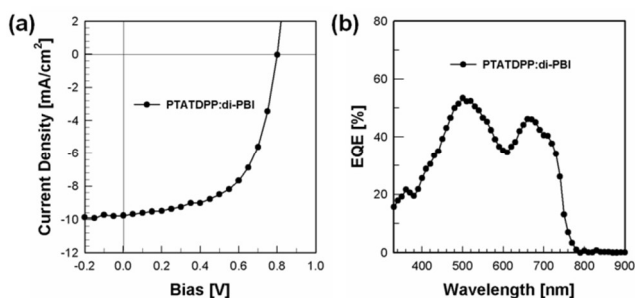


**Fig. 7** (a) *J*-*V* curve and (b) EQE spectra of non-fullerene PSC device fabricated from PTATDPP:di-PBI blend.

the promising photovoltaic performance over 4% PCE with decent photovoltaic parameters ( $V_{OC}$ ,  $J_{SC}$  and FF) suggests that PTATDPP can be used as a universal donor material compatible with various electron acceptors for high performance PSCs.

## 5 Conclusions

We have designed and synthesized two anthracene-based low band-gap copolymers, PTATDPP and PTAFDPP. Since TA unit has highly conjugated 2-D structure with weak electron-donating nature, the copolymer composed of TA and DPP units shows relatively low band-gap, low-lying HOMO energy level, high crystallinity, and efficient charge transporting characteristics. The PSCs fabricated from PTATDPP and PTAFDPP with PC<sub>71</sub>BM exhibit PCEs as high as 7.02% and 5.22%, respectively. Furthermore, PTATDPP shows a promising PCE of 4.23% when a non-fullerene acceptor (di-PBI) is used as an electron acceptor material for PSC device. These results not only demonstrate that thienyl-substituted anthracene is a very promising building block as an electron-donating unit of low band-gap polymers for high performance PSCs but also PTATDPP can be used as a universal electron donor material compatible with various electron acceptor materials in PSCs.

## Experimental

### Materials

*5,5'-(2,6-dibromoanthracene-9,10-diyl)bis(2-(2-ethylhexyl)thiophene) (M1)*: 2 mL of *n*-BuLi solution (2.5 M, 5.0 mmol) was slowly added to a solution of 1.0 g of 2-(2-ethylhexyl)thiophene (5.1 mmol) at 0 °C. After the solution was stirred for 30 min at room temperature, 350 mg of 2,6-dibromo-9,10-anthraquinone (0.96 mmol) was added and the solution was then further stirred for 30 min at room temperature. A mixture of 1.1 g of SnCl<sub>2</sub>·2H<sub>2</sub>O (4.9 mmol) in 10% HCl (10 mL) was then added to the solution and the mixture was stirred for additional 2 h. After the reaction was quenched by pouring the mixture into ice water, the organic layer was extracted with 20 mL of methylene chloride (2 times) and then the organic phase was dried over MgSO<sub>4</sub>. After the solvent was evaporated, the crude product was purified by column chromatography on silica gel using hexane as an eluent yielding pure product of **M1** as yellow solid. (500 mg, Y = 70%) <sup>1</sup>H NMR (300 MHz, CDCl<sub>3</sub>, δ): 8.06 (s, 2H, Ar H), 7.78 (d, 2H, ArH), 7.45 (d, 2H, ArH), 6.97 (dd, 4H), 2.9 (d, 4H), 1.71 (m, 2H), 1.4–1.5 (m, 16H), 0.95 (m, 12H); <sup>13</sup>C NMR (100 MHz, CDCl<sub>3</sub>, δ): 145.5, 129.9, 128.1, 126.3, 125.7, 122.8, 120.0, 119.3, 47.6, 34.1, 32.2, 30.0, 23.2, 26.5, 22.0, 12.1. Anal. Calcd for C<sub>38</sub>H<sub>44</sub>Br<sub>2</sub>S<sub>2</sub>: C 62.98, H 6.12, S 8.85. Found: C 62.95, H 6.17, S 8.81. GC MS = 722.2 (M<sup>+</sup>)

*Synthesis of TDPP*: TDPP was synthesized as the procedure reported in the literature.<sup>22</sup> <sup>1</sup>H NMR (300 MHz, CDCl<sub>3</sub>, δ): 8.92 (d, 2H), 7.63 (d, 2H), 7.27 (d, 2H), 4.05 (m, 4H), 1.56 (m, 2H), 1.4–1.3 (m, 32H), 0.87 (m, 12H).

*Synthesis of FDPP*: FDPP was synthesized as the procedure reported in the literature.<sup>23</sup> <sup>1</sup>H NMR (300 MHz, CDCl<sub>3</sub>, δ): 8.30 (d, 2H), 7.60 (d, 2H), 6.67 (dd, 2H), 4.02 (d, 4H), 1.73 (m, 2H), 1.3–1.2 (m, 32H), 0.95–0.85 (m, 12H).

*Synthesis of M2*: Freshly prepared lithium diisopropyl amine solution in THF (4 mmol) was slowly added to the solution of

640 mg of TDPP (1 mmol) and 750 mg of 2-isopropoxy-4,4,5,5-tetramethyl-1,3,2-dioxaborolane (4 mmol) in 30 mL of anhydrous THF at –78 °C. After the solution was stirred for 30 min, the solution was further stirred for 2 h at 0 °C and then the reaction was quenched by addition of 30 mL HCL solution (1 M). The organic phase was extracted using methylene chloride twice, and the solvent was dried by MgSO<sub>4</sub>. After the solvent was evaporated, the crude product was recrystallized by acetone/hexane mixture twice yielding pure product as purple solid. (550 mg, Y = 62%) <sup>1</sup>H NMR (300 MHz, CDCl<sub>3</sub>, δ): 8.89 (d, 2H), 7.71 (d, 2H), 4.05 (d, 4H), 1.89 (m, 2H), 1.5–1.2 (m, 56H), 0.85 (m, 12H). Anal. Calcd for C<sub>50</sub>H<sub>78</sub>B<sub>2</sub>N<sub>2</sub>O<sub>6</sub>S<sub>2</sub>: C 67.56, H 8.84, N 3.15, S 7.21. Found: C 67.53, H 8.78, N 3.21. GC MS = 888.6 (M<sup>+</sup>)

*Synthesis of M3*: **M3** was prepared as the similar method to the preparation of **M2** except for the use of 600 mg of FDPP (1 mmol) instead of TDPP. (440 mg, Y = 51%) <sup>1</sup>H NMR (300 MHz, CDCl<sub>3</sub>, δ): 8.33 (d, 2H), 7.25 (d, 2H), 4.11 (d, 4H), 1.85 (m, 2H), 1.3–1.2 (m, 56H), 0.85 (m, 12H). Anal. Calcd for C<sub>50</sub>H<sub>78</sub>B<sub>2</sub>N<sub>2</sub>O<sub>8</sub>: C 70.09, H 9.18, N 3.27, O 14.94. Found: C 70.00, H 9.21, N 3.21. GC MS = 856.6 (M<sup>+</sup>)

*Synthesis of PTATDPP*: To a mixture of **M1** (100 mg, 0.138 mmol) and **M2** (122.7 mg, 0.138 mmol) in 4 mL of toluene and 2 mL of K<sub>2</sub>CO<sub>3</sub> solution (2M in H<sub>2</sub>O), 5 mg of Pd(PPh<sub>3</sub>)<sub>4</sub> was added and the mixture was degassed for 30 min. After the solution was refluxed under N<sub>2</sub> atmosphere for 3 day, the reaction (polymerization) was quenched by end-capping using 2-bromothiophene (2.3 mg, 0.014 mmol) and 2-tributylstanylthiophene (10 mg, 0.027 mmol) successively. After cooling down to room temperature, the solution was precipitated in methanol/water mixture. The solid (precipitate) was further purified by Soxhlet extraction successively with methanol, acetone, hexane, and then chloroform. Finally the chloroform fraction was concentrated, and then precipitated in methanol. The dark purple solid was obtained after filtering by PTFE filter. (Y = 80%) Mn/Mw = 47.2 kDa/99.0 kDa.

*Synthesis of PTAFDPP*: PTAFDPP was prepared as the similar method to the preparation of PTATDPP except for using 118.2 mg of **M3** instead of **M2**. The dark purple solid was obtained after filtering by PTFE filter. (Y = 82%) M<sub>n</sub>/M<sub>w</sub> = 32.6 kDa/81.7 kDa.

### Fabrication of photovoltaic devices

Photovoltaic cells were fabricated with a conventional architecture of ITO/PEDOT:PSS/polymer:PC<sub>71</sub>BM/Ca/Al and an inverted architecture of ITO/ZnO/polymer:PC<sub>71</sub>BM/MoO<sub>3</sub>/Ag. The patterned indium tin oxide (ITO) glass was cleaned in an ultrasonic bath of acetone and isopropanol, and treated in ultraviolet-ozone chamber for 30 min. For conventional device architecture, 40 nm of poly(3,4-thylenedioxythiophene):poly(styrene sulfonate) (PEDOT:PSS, Clevios P VP AI 4083) was spin-coated onto the ITO glass and baked at 150 °C for 30 min. For the inverted device, 30 nm of sol-gel driven ZnO film was spin-coated onto the ITO glass and baked at 200 °C for 120 min. *o*-Dichlorobenzene solution (2 wt%) of PTATDPP (or PTAFDPP) and PC<sub>71</sub>BM (Nano-C) was subsequently spin-coated on the top of PEDOT:PSS or ZnO coated ITO glass as an active layer at 90 nm thickness. After drying the active layer, Ca (20 nm) and Al (100 nm) or MoO<sub>3</sub> (10 nm) and Ag (100 nm) were

thermally evaporated under high vacuum ( $<10^{-6}$  Pa) as a metal cathode for conventional and inverted devices, respectively. For non-fullerene solar cell device, the solution (3 wt% in *o*-dichlorobenzene with 1.5 vol% of 1,8-diiodooctane) of PTATDPP and di-PBI (1:2 weight ratio) was used for spin-coating of active layer. The active area of device was 4 mm<sup>2</sup> as determined by shadow mask. The PSC device was characterized in N<sub>2</sub> atmosphere under 100 mW·cm<sup>2</sup> (AM1.5G) irradiation using an Oriel Xe arc lamp coupled with a Keithley 4200 source measurement unit. The solar simulator light intensity was calibrated with an NREL certified Si photodiode with a KG5 optical filter. The incident photon-to-current efficiency (IPCE) of the solar cell device was measured using a lock-in amplifier with a current preamplifier under short circuit current state with illumination of monochromatic light (K3100, McScience Co.).

## Acknowledgements

The authors thank the Ministry of Education, Korea for financial support through the Global Research Laboratory (GRL) program.

## Notes and references

<sup>20</sup> <sup>a</sup>Department of Materials Science and Engineering, Seoul National University, 1 Gwanak-ro, Gwanak-gu, Seoul 151-744, Korea. Fax: +82 2 876 6086; Tel: +82 2 880 7192; E-mail: whjpoly@smu.ac.kr

†Electronic Supplementary Information (ESI) available: Characterization, photoluminescence, device optimization data. See DOI: 10.1039/b000000x/

- 1 C. J. Brabec, N. S. Sariciftci, J. C. Hummelen, *Adv. Funct. Mater.*, 2011, **11**, 15–26.
- 2 J. J. M. Halls, C. A. Walsh, N. C. Greenham, E. A. Marseglla, R. H. Friend, S. C. Moratti, A. B. Holmes, *Nature*, 1995, **376**, 498–500.
- 3 G. Yu, A. J. Heeger, *J. Appl. Phys.*, 1995, **78**, 4510–4515.
- 4 Y. Kim, S. Cook, S. M. Tuladhar, S. A. Choulis, J. Nelson, J. R. Durrant, D. D. C. Bradley, M. Giles, I. McCulloch, C.-S. Ha, M. Ree, *Nat. Mater.*, 2006, **5**, 197–203.
- 5 G. Dennler, M. C. Scharber, C. J. Brabec, *Adv. Mater.*, 2009, **21**, 1323–1338.
- 6 S. H. Park, A. Roy, S. Beaupre, S. Cho, N. Coates, J. S. Moon, D. Moses, M. Leclerc, K. Lee, A. J. Heeger, *Nat. Photonics*, 2009, **3**, 297–302.
- 7 Y. Liang, Z. Xu, J. Xia, S.-T. Tsai, Y. Wu, G. Li, C. Ray, L. Yu, *Adv. Mater.*, 2010, **22**, E135–E138.
- 8 Y. Huang, X. Guo, F. Liu, L. J. Huo, Y. N. Chen, T. P. Russell, C. C. Han, Y. F. Li, J. H. Hou, *Adv. Mater.*, 2010, **24**, 3383–3389.
- 9 S. C. Price, A. C. Stuart, L. Q. Yang, H. X. Zhou, W. You, *J. Am. Chem. Soc.*, 2011, **133**, 4625–4631.
- 10 C. M. Amb, S. Chen, K. R. Graham, J. Subbiah, C. E. Small, F. So, J. R. Reynolds, *J. Am. Chem. Soc.*, 2011, **133**, 10062–10065.
- 11 G. Li, R. Zhu, Y. Yang, *Nat. Photon.*, 2012, **6**, 153–161.
- 12 L.-M. Chen, Z. Hong, G. Li, Y. Yang, *Adv. Mater.*, 2009, **21**, 1434–1449.
- 13 Y. Liang, Y. Wu, D. Feng, S. T. Tsai, H. J. Son, G. Li, L. Yu, *J. Am. Chem. Soc.*, 2009, **131**, 56–57.
- 14 F. Huang, K. S. Chen, H. L. Yip, S. K. Hau, O. Acton, Y. Zhang, J. Luo, A. K.-Y. Jen, *J. Am. Chem. Soc.*, 2009, **131**, 13886–13887.
- 15 Y. Zhang, S. K. Hau, H. L. Yip, Y. Sun, O. Acton, A. K.-Y. Jen, *Chem. Mater.*, 2010, **22**, 2696–2698.
- 16 C. E. Small, S. Chen, J. Subbiah, C. M. Amb, S. W. Tsang, T. H. Lai, J. R. Reynolds, F. So, *Nat. Photon.*, 2012, **6**, 115–120.
- 17 L. Dou, J. You, J. Yang, C.-C. Chen, Y. He, S. Murase, T. Moriarty, K. Emery, G. Li, Y. Yang, *Nat. Photon.*, 2012, **6**, 180–185.
- 18 J. J. Intemann, K. Yao, Y.-X. Li, H.-L. Yip, Y.-X. Xu, P.-W. Liang, C.-C. Chueh, F.-Z. Ding, X. Yang, X. Li, Y. Chen, A. K.-Y. Jen, *Adv. Funct. Mater.*, 2014, **24**, 1465–1473.
- 19 F. Liu, Y. Gu, C. Wang, W. Zhao, D. Chen, A. L. Briseno, T. P. Russell, *Adv. Mater.*, 2012, **24**, 3947–3951.
- 20 J. W. Jung, F. Liu, T. P. Russell, W. H. Jo, *Chem. Commun.*, 2013, **49**, 8495–8497.
- 21 J. W. Jung, F. Liu, T. P. Russell, W. H. Jo, *Energy Environ. Sci.*, 2012, **5**, 6857–6861.
- 22 A. T. Yiu, P. M. Beaujuge, O. P. Lee, C. H. Woo, M. F. Toney, J. M. J. Frechet, *J. Am. Chem. Soc.*, 2012, **134**, 2180–2185.
- 23 M. Kaur, D. S. Yang, J. Shin, T. W. Lee, K. Choi, M. J. Cho, D. H. Choi, *Chem. Commun.*, 2013, **49**, 5495–5497.
- 24 K. H. Hendriks, G. H. L. Heintges, V. S. Gevaerts, M. M. Wienk, R. A. J. Janssen, *Angew. Chem., Int. Ed.*, 2013, **52**, 8341–8344.
- 25 R. S. Ashraf, I. Meager, M. Nikolka, M. Kirkus, M. Planells, B. C. Schroeder, S. Holliday, M. Hurhangee, C. B. Nielsen, H. Sirringhaus, I. McCulloch, *J. Am. Chem. Soc.*, 2015, **137**, 1314–1321.
- 26 H. Bronstein, Z. Y. Chen, R. S. Ashraf, W. M. Zhang, J. P. Du, J. R. Durrant, P. S. Tuladhar, K. Song, S. E. Watkins, Y. Geerts, M. M. Wienk, R. A. J. Janssen, T. Anthopoulos, H. Sirringhaus, M. Heeney, I. McCulloch, *J. Am. Chem. Soc.*, 2011, **133**, 3272–3275.
- 27 L. T. Dou, W.-H. Chang, J. Gao, C.-C. Chen, J. B. You, Y. Yang, *Adv. Mater.*, 2013, **25**, 825–831.
- 28 W. Li, K. H. Hendriks, A. Furlan, W. S. C. Roelofs, M. M. Wienk, R. A. J. Janssen, *J. Am. Chem. Soc.*, 2013, **135**, 18942–18948.
- 29 J.-H. Kim, M. Lee, H. Yang, D.-H. Hwang, *J. Mater. Chem. A*, 2014, **2**, 6348–6352.
- 30 J. C. Bijleveld, V. S. Gevaerts, D. Di Nuzzo, M. Turbiez, S. G. J. Mathijssen, D. M. de Leeuw, M. M. Wienk, R. A. J. Janssen, *Adv. Mater.*, 2010, **22**, E242–E246.
- 31 P. Sonar, S. P. Singh, Y. Li, Z.-E. Ooi, T.-J. Ha, I. Wong, M. S. Soh, A. Dodabalapur, *Energy Environ. Sci.*, 2011, **4**, 2288–2296.
- 32 P. Sonar, S. P. Singh, E. L. Williams, Y. Li, M. S. Soh, A. Dodabalapur, *J. Mater. Chem.*, 2012, **22**, 4425–4435.
- 33 J. W. Jung, F. Liu, T. P. Russell, W. H. Jo, *Adv. Energy Mater.*, 2015, DOI: 10.1002/aenm.201500065.
- 34 L. Ye, S. Zhang, L. Huo, M. Zhang, J. Hou, *Acc. Chem. Res.*, 2014, **47**, 1595–1603.
- 35 C. Liu, W. Cai, X. Guan, C. Duan, Q. Xue, L. Ying, F. Huang, Y. Cao, *Polym. Chem.*, 2013, **4**, 3949–3958.
- 36 M. S. Almeataq, H. Yi, S. Al-Faifi, A. A. B. Alghamdi, A. Iraqi, N. W. Scarratt, T. Wang, D. G. Lidzey, *Chem. Commun.*, 2013, **49**, 2252–2254.
- 37 (a) L. Huo, J. Hou, H.-Y. Chen, S. Zhang, Y. Jiang, T. L. Chen, Y. Yang, *Macromolecules*, 2009, **42**, 6564–6571; (b) X. M. Jiang, R. Österbacka, O. Korovyanko, C. P. An, B. Horovitz, R. A. J. Janssen, Z. V. Vardeny, *Adv. Funct. Mater.*, 2002, **12**, 587–597.
- 38 (a) W. Jiang, L. Ye, X. Li, C. Xiao, F. Tan, W. Zhao, J. Hou, Z. Wang, *Chem. Commun.*, 2014, **50**, 1024–1026; (b) Y. Zang, C.-Z. Li, C.-C. Chueh, S. T. Williams, W. Jiang, Z. Wang, J.-S. Yu, A. K. Y. Jen, *Adv. Mater.*, 2014, **26**, 5708–5714.
- 39 J. D. Servaites, M. A. Ratner, T. J. Marks, *Energy Environ. Sci.*, 2011, **4**, 4410–4422.